Organic LETTERS

Letter

pubs.acs.org/OrgLett

# Self-Assembly of Tetraphenylethene-Based [2]Catenane Driven by Acid−Base-Controllable Molecular Switching and Its Enabled Aggregation-Induced Emission

Mandapati V. Ramakrishnam Raju and Hong-Cheu Lin*

Department of Materials Science and Engineering, National Chiao Tung University, Hsinchu 30049, Taiwan

Supporting Information

**ABSTRACT:** A novel [2]catenane **2-C** based on the tetraphenylethene (TPE) and orthogonal H-bonded cleft was successfully constructed. VT-NMR and TEM measurements demonstrate that **2-C** could be self-assembled to induce an enabled aggregation-induced emission (AIE) in aqueous solution and solid state owing to its TPE unit as well as present unique acid−base controllable and reversible supramolecular self-assembled nanosuperstructures by interplay of a wide range of noncovalent interactions.

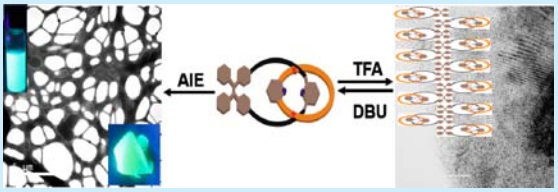


In the realm of supramolecular chemistry, mechanically interlocked molecules (MIMs) of macrocycles, such as catenanes, knots, and rotaxanes, have long been carved as an indelible field, owing to their indispensable roles in constructing nanomachines, switches, and drug delivery vehicles.[1−3] Precise understanding and control of supramolecular interactions, such as H-bonding, anion−$\pi$, C−H−$\pi$, electrostatic, and $\pi-\pi$ stacking interactions between the entwined macrocycles are pivotal in synthesizing catenanes rationally, as this process is entropically disfavored. However, the emergence of template-directed synthetic protocols in designing MIMs are allowed to realize complex architectures.[4] Stoddart et al. have extensively researched bistable catenanes via $\pi$-donor/$\pi$-acceptor self-assembling approaches.[5] Beer et al. developed an anion-templating protocol for the construction of MIMs.[6] Even spontaneous quantitative catenane formation without an auxiliary template was realized by Fujita's group with the aid of hydrophobic interactions between two macrocycles.[7]

The quest continues for creating ideal architectures that work under deliberate quelling conditions in aqueous media, where most biological processes are favorable in their functioning and are studied by supramolecular chemists.[1,8] Recently, a few examples of MIM-based molecular switches have been reported to be operational in aqueous media.[9] However, an understanding of self-assembly with controllable photophysical characteristics of [2]catenane is still needed at the molecular level.

Since the discovery of abnormal photophysical phenomena of AIE by Tang's group,[10] myriad molecular probes for detecting wide ranges of biomolecules were reported.[11] Conventionally, these probes have relied on the restriction of intramolecular rotations (RIR) of phenyl groups in AIE active units as suggested by previous reports.[12] Recently, Tang's group has demonstrated the restriction of intramolecular motions by forming a host−guest inclusion complex of TPE-functionalized $\beta$-cyclodextrin (CD).[13] Zheng et al. reported that the aggregation emission of a monomer containing an amphiphilic TPE moiety could be tuned by its inclusion complex with $\gamma$-CD.[14] However, it remains a challenge to build a mechanically interlocked molecule which could be fluorescence-active by an enabled RIR process in an aggregated state. Thus, from the viewpoint of creating a unique self-assembled functional MIM, the orthogonal H-bonded [2]catenane unit with an intact AIE active luminogen might provide an interesting paradigm. However, to the best of our knowledge, such a system has not been explored yet. To mimic this idea, we need an ideal topological cavity formed in situ by virtue of mechanical bonding with a preorganized and yet RIR-active aromatic unit in the aggregation state.

To unfold such an astonishing example, herein we have designed and synthesized a prototype [2]catenane by ring-closing metathesis[15] on a [2]pseudorotaxane formed between a macrocycle **T1** via a square-planar Pd(II) metal template approach[16] as shown in Scheme 1. Indeed, all previous interlocked molecules reported by this metal template approach were neither functionality- nor property-enriched systems at the molecular level. For a detailed synthesis of macrocycle **T1** (Scheme S1) and other characterization data see the Supporting Information. [2]Catenane **2-C** presented an enriched AIE capability in contrast to its precursors **2**, **T1**, and **TPd** in solution and AIE aggregation states (in THF/water mixtures at water fraction $f_w$ = 90%). Furthermore, **2-C** showed unprecedented controllable and reversible self-assembled nanostructures under acid−base and in the AIE state.

To verify the effective entwining between two macrocycles, $^1$H NMR spectra of **2-C**, 2,6-dicarbaxamidopyridyl macrocycle (**M**), TPE macrocycle (**T1**), and 1:1 mixture of **T1** and **M** were compared in $CDCl_3$ as shown in Figure 1. Upfield shifts for pyridyl protons (**a** and **b**) in **M** and pyridyl protons (**A** and **B**) in **T1** along with a 1.2 ppm downfield shift for the amide proton (**c**) in **M** were noticed. Moreover, the upfield shifts for aromatic

**Received:** August 30, 2014
**Published:** October 24, 2014





dx.doi.org/10.1021/ol5025629 | Org. Lett. 2014, 16, 5564−5567

**Scheme 1. Synthesis of [2]Catenane 2-C**

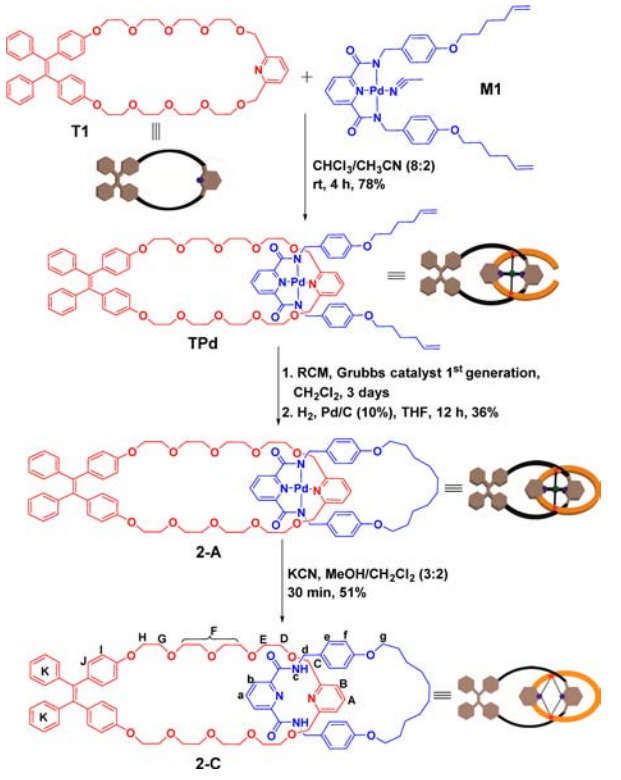


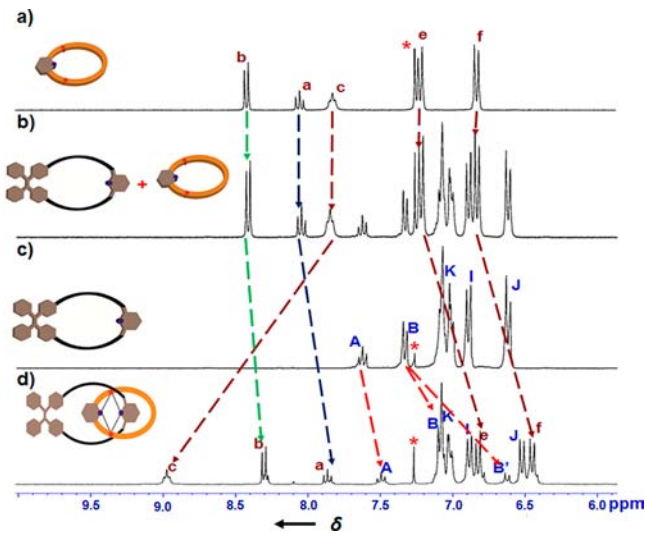


**Figure 1.** $^1$H NMR spectra ($CDCl_3$, 300 MHz, 298 K): (a) macrocycle **M**, (b) 1:1 mixture of **M** and **T1**, (c) **T1**, and (d) [2]catenane **2-C**. The assignments correspond to the lettering shown in Scheme 1. Asterisks correspond to $CHCl_3$. Capital and lowercase alphabetical labeling denotes the TPE macrocycle **T1** and macrocycle **M**, respectively.

protons (**e** and **f**) of **M** denoted the strong aromatic shielding effect between aromatic units in [2]catenane **2-C**, which indicated the existence of an overwhelming mechanical interlocking between the two wheels via an orthogonal bifurcated pyridine−pyridine H-bonded interactions.

Furthermore, noticeable upfield shifts of the ethylene glycol unit along with downfield shifts of **T1** pyridyl protons in relative polar solvent $d_6$-DMSO suggested that the macrocycle **M** was translocated to glycol unit as the H-bonding basicity was increased along with a coupled solvophobic effect (Figure S1b, Supporting Information).[16f] $^1$H spectroscopy analysis of **2-C** (Figure S1a, Supporting Information) with broad and upfield shifts in $D_2O$ denoted that the bifurcated H-bonding between two wheels was disrupted and two wheels were translocating to each other at molecular level with peak broadening owing to the aggregation of TPE unit in **2-C**.

To make use of in situ topological cavities of **2-C** formed upon demetalation of **2-A**,[17] we further studied host−guest properties of **2-C** and **T1** in the presence of trifluoroacetic acid (TFA) and their nature of dynamic self-assembly by performing a series of $^1$H and variable temperature (VT)-NMR experiments. As shown in Figure S2 (Supporting Information), the marked downfield shifts for wheel amide protons **c** and pyridyl protons **A** and **B** during the titration of **2-C** with TFA clearly denoted that TFA was deprotonated and induced to form a strong H-bonded complex with the resulting trifluorocarboxylate anion. Moreover, noticeable downfield shits for pyridyl protons **A**, **B**, and **C** of **T1** upon titrating with TFA (see Figure S3, Supporting Information) attested the deprotonation of TFA by pyridyl unit in **T1**. As depicted in Figures S4 and S5 (Supporting Information), the acid-mediated[16g] host−guest interactions of both **2-C** and **T1** were completely reversible upon adding base 1,8-diazabicyclo[5.4.0]undec-7-ene (DBU).

When the temperature cooled to 258 K for the free **2-C** sample, we noticed split resonances for amide protons **c** along with broad and marginal downfield shifts for other aromatic protons (Figure 2). However, when the sample was heated to

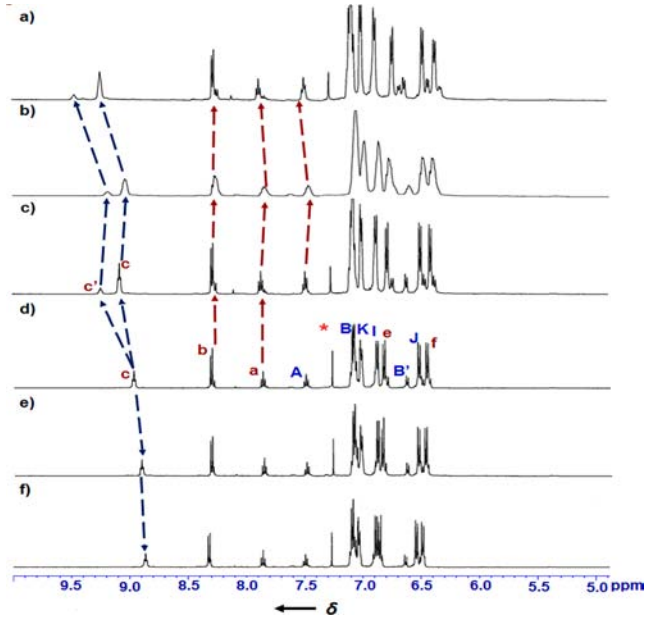


**Figure 2.** VT-NMR ($CDCl_3$, 500 MHz) stock plot of [2]catenane **2-C** (3 mM): (a) at 238 K, (b) 258 K, (c) 273 K, (d) 298 K, (e) 313 K, and (f) 323 K, respectively. The assignments correspond to the lettering shown in Scheme 1. Asterisks correspond to the $CHCl_3$.

323 K close to the boiling point of $CDCl_3$, we noticed a marginal upfield shifts for aromatic protons. Similar VT-NMR tends were observed even in the case of complex **2-C-TFA** along with the coalescence for the complex protons as illustrated in Figure S6 (Supporting Information). The observed VT-NMR trends of free **2-C** and complex **2-C-TFA** indicated pirouetting-like conformational changes of macrocycles abetted by amide rotamerization of **2-C** and by additional intercomponent


dx.doi.org/10.1021/ol5025629 | Org. Lett. 2014, 16, 5564−5567

anion-$\pi$ interactions of **2-C-TFA**. To our delight, we observed a trivial and persisted NMR resonance peaks for free TPE macrocycle **T1** as depicted in Figure S7 (Supporting Information) during VT-NMR measurements.

The significant $^1$H NMR spectral changes for **2-C** at low temperatures in contrast to the free **T1** clearly demonstrated that mechanical interlocking effectively controlling the RIR process owing to its inherent conformational changes at the molecular level than those of free macrocycle **T1.** Thus, the relative population of co-conformational switching by adding water and acid in [2]catenane (owing to the translational isomerism) has a profound effect on controlling the phenyl ring rotation of TPE unit in **2-C** than those of free macrocycle **T1**.

Moreover, complex **T1-TFA** showed initial downfield shifts for pyridyl protons **A** and **B** at 298 K in comparison with the free **T1**. However, when the sample was cooled down to 238 K we noticed broad and upfield shifts for pyridyl protons along with uncomplexed-precipitation of TFA as depicted in Figure S8 (Supporting Information). Thus, these results affirmed that the thermally controllable dynamic self-assembly of **2-C** and complex **2-C-TFA** were distinctive from free macrocycle **T1** and complex **T1-TFA**. Furthermore, we attributed these observation to an augmented positive cooperative self-assembly of **2-C**, which was coupled with strong $\pi-\pi$, anion$-\pi$, hydrophobic, and thermally preserved orthogonal H-bonded interactions in empowering the effective RIR process of **2-C**.

How do TPE molecules behave if we can interlock them as a functional [2]catenane **2-C**? Will mechanical bonding boost the AIE of an interlocked molecule? Intrigued by these questions, we next sought to investigate the photophysical properties of **2-C** and its precursors in solution and aggregation states. **2-C** showed an absorption maximum at 324 nm corresponding to $\pi-\pi^*$ transition of the molecule and exhibited a weak fluorescence emission band at 379 nm in a dilute THF solution. However, in THF/water mixtures with gradual increments of water contents ($f_w \geq 90\%$) **2-C** exhibited a strong fluorescence emission at 480 nm with a bathochromic shift as shown in Figure 3a,b. The

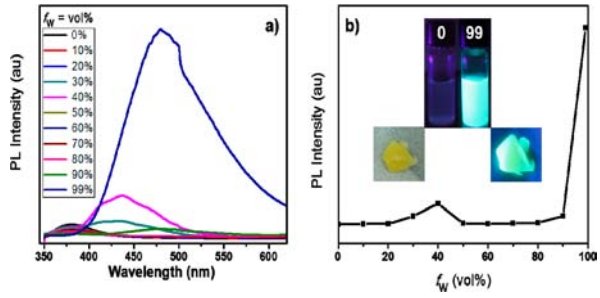


**Figure 3.** PL spectra of (a) **2-C** (10 $\mu$M) in THF/water mixtures with different water fractions ($f_w$ 0–99 vol %), (b) emission changes at 480 nm of **2-C** during the gradual addition of water fractions. $\lambda_{ex}$ = 324 nm. Inset (b): photos of **2-C** in THF/water mixtures ($f_w$ = 0 and 99%) and solid samples taken under day light (naked eye observation) and UV illuminations.

narrower AIE window of **2-C** could be attributed to its dichotomous solubility in THF/water mixture. The distinctive emission behaviors of **2-C** at low and high water fractions indicated **2-C** molecules tend to aggregate as the effective restriction of RIR process and eventually blocked their nonradiation decay pathways. Thus, **2-C** emitted strongly in its aggregation state and attested its anticipated AIE capability.

Even though both macrocycle **T1** and TPE intermediate **2** exhibited AIE capabilities, their responses were trivial and distinctive from **2-C** under working conditions as revealed in parts a and b, respectively, of Figure S9a (Supporting Information), respectively. Moreover, the precursor-metalated [2]pseudorotaxane **TPd** showed negligible emission behavior under similar conditions as shown in Figure S10 (Supporting Information). These observations were plugged to an effective annihilation of low-frequency excitons via nonradiative decay pathways owing to their metal coordination.

To further evaluate the AIE properties of [2]catenane **2-C** and its precursors (**2**, **T1**, and **TPd**), their quantum yields are calculated in solution and aggregation states and summarized in Table S1 (Supporting Information). In contrast to its precursors, the relative high quantum yield of **2-C** upon addition of water was clearly denoted by an effective blocking of the nonradiative decay pathway by controlling phenyl motions of TPE unit.

We probed further scanning and transmission electron microscopies[18] to evaluate the self-assembled structures of topological luminogens. As shown in Figure 4a, TEM micro-

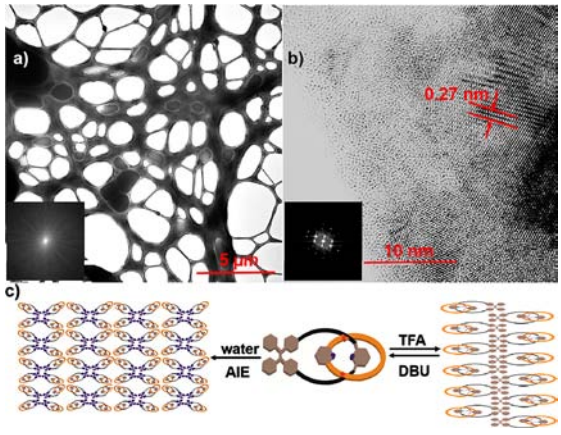


**Figure 4.** HR-TEM images of self-assembled structures of **2-C** formed in THF/water mixture (a) aggregation state at $f_w$ = 90% and (b) in the protonated state with the addition of TFA in THF. Insets: (a, b) reduced Fourier transformed patterns of **2-C** in their respective states. Scale bars in a and b are 5 $\mu$M and 10 nm, respectively. (c) Plausible self-assembly mechanism of **2-C** under pH (right) and AIE (left) triggers.

graphs of **2-C** showed an uniquely aggregated nanostructure drawn from a THF/water mixture at $f_w$ = 90%. However, Figure 4b presented hierarchical self-assembled nanochannel structures in the protonated state. As shown in the insets of Figure 4a,b for their respective states, the measured dark/light periodicity (with an average spacing of 0.27 nm) from Fourier analysis suggested a crystalline nanochannel structure in contrast to amorphous microaggregates to induce AIE behavior. SEM analyses of **2-C**, as demonstrated in Figure S11a,b (Supporting Information) under AIE and pH triggers, further attested the unique self-assembly of [2]catenane.

Moreover, the amplified supramolecular self-assemblies of **2-C** were successfully demonstrated by the observed dissimilar electron micrographic patterns of macrocycle **T1** under AIE and pH stimuli in parts a and b, respectively, of Figure S12 (Supporting Information). In addition, dynamic light scattering (DLS) measurements revealed an average hydrodynamic diameter of 296 nm for **2-C** formed in the THF/water mixture at $f_w$ = 90% as illustrated in Figure S13a (Supporting Information). However, we noticed an average hydrodynamic


dx.doi.org/10.1021/ol5025629 | *Org. Lett.* 2014, 16, 5564–5567

diameter of 180 nm in the aggregation of **T1** (see Figure S13b, Supporting Information), but we could not find any detectable particle aggregations in all other samples.[19] These results were consistent with the above VT-NMR and photophysical measurements. Therefore, **2-C** could have evolved via folded geometry of interlocked interlocked luminogens due to $\pi-\pi$ stackings and hydrophobic interactions in the AIE state as shown in Figure 4c. Moreover, the protonated state of self-assembly in **2-C** in a layer-by-layer fashion was governed by a dynamic organization process of interlocked luminogens to avoid local electrostatic repulsions between protonated wheel and concomitant H-bonded complex.

With unique topological cavities constructed in situ by virtue of mechanical bonding in [2]catenane, **2-C** is rendered AIE-active by its interlocked TPE unit, which establishes an unprecedented example of functional MIMs. Abetted by its orthogonal H-bonds, $\pi-\pi$ stackings, C−H−$\pi$ interactions, it shows unique self-assembled structures formed under pH and aqueous triggers. Furthermore, an augmented AIE phenomenon of **2-C** occurs in contrast to its precursors in this study. Further studies to appreciate the unique dynamics of this novel catenane at the molecular level are being pursued in our laboratory. We believe the results could open the door to promising applications for the construction of more complex and yet bright multifunctional MIMs.

## ■ ASSOCIATED CONTENT

### Supporting Information

Synthetic procedures, supporting figures, and spectral data. This material is available free of charge via the Internet at http://pubs.acs.org.

## ■ AUTHOR INFORMATION


### Corresponding Author

*E-mail: linhc@mail.nctu.edu.


### Notes

The authors declare no competing financial interest.

## ■ ACKNOWLEDGMENTS

This project was financially supported by the National Science Council of Taiwan (ROC) through funding no. NSC 101-2113-M-009-013-MY2.

## ■ REFERENCES


(1) Coskun, A.; Spruell, J. M.; Barin, G.; Dichtel, W. R.; Flood, A. H.; Botros, Y. Y.; Stoddart, J. F. *Chem. Soc. Rev.* **2012**, *41*, 4827−4859.

(2) (a) Kay, E. R.; Leigh, D. A.; Zerbetto, F. *Angew. Chem., Int. Ed.* **2007**, *46*, 72−191. (b) Balzani, V.; Credi, A.; Venturi, M. *Molecular Devices and Machines: Concepts and Perspectives for the Nanoworld*, 2nd ed.; Wiley-VCH: Weinheim, 2008.

(3) (a) Li, Z.; Barnes, J. C.; Bosoy, A.; Stoddart, J. F.; Zink, J. I. *Chem. Soc. Rev.* **2012**, *41*, 2590−2605. (b) Yong, Y. W.; Song, Y. L.; Song, N. *Acc. Chem. Res.* **2014**, *47*, 1950−1960.

(4) (a) Lim, C. W.; Sakamoto, S.; Yamaguchi, K.; Hong, J.-I. *Org. Lett.* **2004**, *6*, 1079−1082. (b) Gamez, P.; Mooibroek, T. J.; Teat, S. J.; Reedijk, J. *Acc. Chem. Res.* **2007**, *40*, 435−444. (c) Blight, B. A.; Campbell, C. J.; Leigh, D. A.; McBurney, R. T. *Angew. Chem., Int. Ed.* **2011**, *50*, 9260−9327.

(5) Fahrenbach, A. C.; Bruns, C. J.; Li, H.; Trabolsi, A.; Coskun, A.; Stoddart, J. F. *Acc. Chem. Res.* **2014**, *47*, 482−493.

(6) Sambrook, M. R.; Beer, P. D.; Wisner, J. A.; Paul, R. L.; Cowley, A. R. *J. Am. Chem. Soc.* **2004**, *126*, 15364−15365.

(7) Fujita, M.; Ibrukuro, H.; Hagihara, H.; Ogura, K. *Nature* **1994**, *367*, 720−723.

(8) Coskun, A.; Banaszak, M.; Astumian, R. D.; Stoddart, J. F.; Grzybowski, B. A. *Chem. Soc. Rev.* **2012**, *41*, 19−30.

(9) (a) Fang, L.; Basu, S.; Sue, C. H.; Fahrenbach, A. C.; Stoddart, J. F. *J. Am. Chem. Soc.* **2011**, *133*, 396−399. (b) Fang, L.; Wang, C.; Fahrenbach, A. C.; Trabolsi, A.; Botros, Y. Y.; Stoddart, J. F. *Angew. Chem., Int. Ed.* **2011**, *50*, 1805−1809. (c) Li, H.; Fahrenbach, A. C.; Coskun, A.; Zhu, Z.; Zhao, Y.; Botros, Y. Y.; Sauvage, J. P.; Stoddart, J. F. *Angew. Chem., Int. Ed.* **2011**, *50*, 6782−6788. (d) Forgan, R. S.; Gassensmith, J. J.; Cordes, D. B.; Boyle, M. M.; Hartlieb, K. J.; Friedman, D. C.; Slawin, A. M. Z.; Stoddart, J. F. *J. Am. Chem. Soc.* **2012**, *134*, 17007−17010. (e) Grunder, S.; McGrier, P. L.; Whalley, A. C.; Boyle, M. M.; Stern, C.; Stoddart, J. F. *J. Am. Chem. Soc.* **2013**, *135*, 17691−17694.

(10) Luo, J.; Xie, Z.; Lam, J. W. Y.; Cheng, L.; Qiu, C.; Kwok, H. S.; Zhan, X.; Liu, D.; Zhu, D.; Tang, B. Z. *Chem. Commun.* **2001**, 1740−1741.

(11) (a) Shi, H.; Liu, Z.; Geng, J.; Tang, B. Z.; Liu, B. *J. Am. Chem. Soc.* **2012**, *134*, 9569−9572. (b) Yuan, Y.; Kwok, R. T. K.; Tang, B. Z.; Liu, B. *J. Am. Chem. Soc.* **2014**, *136*, 2546−2554.

(12) (a) Shustova, N. B.; McCarthy, B. D.; Dinca, M. *J. Am. Chem. Soc.* **2011**, *133*, 20126−20129. (b) Hong, Y.; Lam, J. W. Y.; Tang, B. Z. *Chem. Soc. Rev.* **2011**, *40*, 5361−5388. (c) Shustova, N. B.; Ong, T. C.; Cozzolino, A. F.; Michaelis, V. K.; Griffin, R. G.; Dinca, M. *J. Am. Chem. Soc.* **2012**, *134*, 15061−15070.

(13) Liang, G.; Lam, J. W. Y.; Qin, W.; Li, J.; Tang, B. Z. *Chem. Commun.* **2014**, *50*, 1725−1727.

(14) Song, S.; Zheng, H. F.; Li, D. M.; Wang, J. H.; Feng, H. T.; Zhu, Z. H.; Chen, Y. C.; Zheng, Y. S. *Org. Lett.* **2014**, *16*, 2170−2173.

(15) Guidry, E. N.; Cantrill, S. J.; Stoddart, J. F.; Grubs, R. H. *Org. Lett.* **2005**, *7*, 2129−2132.

(16) (a) Fuller, A. M.; Leigh, D. A.; Lusby, P. J.; Oswald, I. D. H.; Parsons, S.; Walker, D. B. *Angew. Chem., Int. Ed.* **2004**, *43*, 3914−3918. (b) Fuller, A. M.; Leigh, D. A.; Lusby, P. J.; Slawin, A. M. Z.; Walker, D. B. *J. Am. Chem. Soc.* **2005**, *127*, 12612−12619. (c) Berna, J.; Crowley, J. D.; Goldup, S. M.; Hanni, K. D.; Lee, A. L.; Leigh, D. A. *Angew. Chem., Int. Ed.* **2007**, *46*, 5709−5713. (d) Liu, Y.; Bruneau, A.; He, Z.; Abliz, Z. *Org. Lett.* **2008**, *10*, 765−768. (e) Leigh, D. A.; Lusby, P. J.; Slawin, A. M. Z.; Walker, D. B. *Chem. Commun.* **2012**, *48*, 5826−5828. (f) Raju, M. V. R.; Lin, H. C. *Org. Lett.* **2013**, *15*, 1274−1277. (g) Raju, M. V. R.; Raghunath, P.; Lin, M. C.; Lin, H. C. *Macromolecules* **2013**, *46*, 6731−6743.

(17) Owing to the close retention factors ($R_f$) of intermediate compound **2-A** and its precursor, the purification of **2-A** with intricate nature was difficult to achieve. However, only a tiny amount of **2-A** containing some impurities was obtained with serendipitous effort, which was eventually utilized for the demetalation step to yield a pure [2]catenane (**2-C**) in assessing chemical homogeneity and key properties of the final compound **2-C** in this study. Additional data files of **2-A**, including $^{1}$H and $^{13}$C NMR with marked impurities as well as an authentic HRMS data, are available in the Supporting Information.

(18) Xu, L.; Jiang, L.; Drecshler, M.; Sun, Y.; Liu, Z.; Huang, J.; Tang, B. Z.; Stuart, M. A. C.; Yan, Y. *J. Am. Chem. Soc.* **2014**, *136*, 1942−1947.

(19) To further appreciate the unique photophysical phenomena and self-assembly nature of [2]catenane (**2-C**) in contrast to its precursors, additional characterizations, such as 2D-diffusion order NMR, IR spectroscopy, UV−vis measurements, and theoretical (DFT) calculations, were conducted and are summarized in the Supporting Information as Figures S14−S19, respectively.